

# Experimental Preparation of Topologically Ordered States via Adiabatic Evolution

Zhihuang Luo<sup>1,2</sup>, Jun Li<sup>2</sup>, Zhaokai Li<sup>1</sup>, Ling-Yan Hung<sup>3,4,5</sup>,\* Yidun Wan<sup>3,4,5,6</sup>,† Xinhua Peng<sup>1,7</sup>,‡ and Jiangfeng Du<sup>1,7</sup>

<sup>1</sup>*Hefei National Laboratory for Physical Sciences at Microscale and Department of Modern Physics,  
University of Science and Technology of China, Hefei, Anhui 230026, China*

<sup>2</sup>*Beijing Computational Science Research Center, Beijing, 100094, China*

<sup>3</sup>*State Key Laboratory of Surface Physics and Department of Physics,  
Fudan University, 220 Handan Road, 200433 Shanghai, China*

<sup>4</sup>*Department of Physics and Center for Field Theory and Particle Physics,  
Fudan University, 220 Handan Road, 200433 Shanghai, China*

<sup>5</sup>*Collaborative Innovation Center of Advanced Microstructures, Nanjing University, Nanjing, 210093, China*

<sup>6</sup>*Perimeter Institute for Theoretical Physics, Waterloo, Ontario N2L 2Y5, Canada and*

<sup>7</sup>*Synergetic Innovation Center of Quantum Information and Quantum Physics,  
University of Science and Technology of China, Hefei, Anhui 230026, China*

Topological orders are a class of exotic states of matter characterized by patterns of long-range entanglement. Certain topologically ordered matter systems are proposed as a potential realization of naturally fault-tolerant quantum computation. Topological orders can arise in two-dimensional spin-lattice models, and here, we engineer the time-dependent Hamiltonian of such a model and prepare a topologically ordered state through adiabatic evolution. The other sectors in the degenerate ground-state space of the model are realized by performing nontrivial closed string operations. Each sector is highly entangled, as shown from the completely reconstructed density matrices. This paves the way towards exploring the properties of topological orders and the application of topological orders in topological quantum memory.

PACS numbers: 03.67.Ac, 03.65.Vf, 76.60.-k

## I. INTRODUCTION

The emergence of topological order in fractional quantum Hall effect has broadened our understanding of phases of matter [1–3]. It manifests that the internal orders of matter are much richer than symmetry-breaking phases. In the framework of Landau theory [4–6], all phases of matter were thought to be characterized by different symmetries and their possible phase transitions were associated with a broken symmetry. Since the different fractional quantum Hall states have exactly same symmetries [3], they are beyond the description of Landau symmetry-breaking theory and cannot be distinguished by local order parameters. Microscopically, topological order corresponds to patterns of long-range entanglement [7]. The topological entanglement entropy can be used as a nonlocal order parameter to identify the topological phases [8, 9].

Topological orders are of basic scientifically interest not only for their topological properties such as fractional quasiparticle statistics [8, 10–12] but also for their profound application in naturally fault-tolerant quantum computation [13–16]. This application mainly relies on the topological robustness of degenerate ground states [10] and their patterns of long-range entanglement [7]. Topologically ordered states can arise as degenerate ground states of certain Hamiltonian of system on a

Riemann surface. Its ground-state degeneracy depends on the genus or holes of the Riemann surface. Because any two orthogonal sectors in ground-state space are connected by non-contractible loop operators, the local perturbations cannot cause the transitions between different sectors. It protects the coherence of information encoded in this manifold. On the other hand, the patterns of long-range entanglement make each sector robust against local perturbations as well. The effects of the former and the latter seem to be error-free similarly for phase flip and bit flip models, respectively. These properties of such systems are attractive for constructing a very robust memory register [17, 18].

Two-dimensional spin-lattice models exhibit topological orders [13, 19, 20]. However, such models usually include many-body interactions that have not been found in naturally physical systems. Without this limitation, Feynman suggested that [21] a well-controlled quantum system can be used for the efficient simulation of other quantum systems and promises to have potential applications in studying detailed quantum phenomenon of inaccessible quantum systems. Quantum simulation could be realized by various physical platforms such as trapped ion [22], superconducting circuit [23], nuclear magnetic resonance (NMR) [24], and so on. There have been a lot of successful demonstrations of quantum simulation in condensed matter physics [25–27], high-energy physics, atomic physics, quantum chemistry [28], and cosmology (see the review of [29] and references therein). Quantum simulation provides a powerful tool to investigate the complex quantum systems exhibiting topological order.

In this Letter, we realize the Hamiltonian of Wen-

\* Lyhung@fudan.edu.cn

† ydwan@fudan.edu.cn

‡ xhpeng@ustc.edu.cn

plaquette spin-lattice model with  $Z_2$  topological orders in an NMR system. There are four-fold degenerate ground states when considering the periodic boundary condition, i.e., on a torus. Following the method proposed by Hamma *et al.* [30], a topologically ordered state is experimentally prepared through adiabatically engineering the time-dependent Hamiltonian and the other sectors in degenerate ground-state manifold are transferred by performing two nontrivial closed string operations. We reconstruct the density matrices for each sector using complete quantum state tomography technology. The results show that each sector exhibits maximum entanglement. It is a central step to prepare topologically ordered states for studying topological quantum phase transition [31], measuring modular matrices [32], constructing robust quantum memory, and so on.

## II. WEN-PLAQUETTE MODEL

The Wen-plaquette model building on an  $N \times N$  square lattice is illustrated in Fig. 1, where each site are placed a spin  $1/2$  [20]. Its Hamiltonian is written as

$$H_{\text{Wen}} = - \sum_{\text{white plaquettes}} X_p - \sum_{\text{yellow plaquettes}} Z_p. \quad (1)$$

Here  $X_p = \prod_{j \in \partial p} \sigma_j^x$ ,  $Z_p = \prod_{j \in \partial p} \sigma_j^z$  are the plaquette operators that act on four spins surrounding a plaquette of  $p$ , and  $\sigma_j^\alpha$ 's stand for pauli operators. This is a exact solvable model because of  $[X_p, Z_{p'}] = 0$  for all  $p$  and  $p'$ . The theory shows that it is equivalent to toric code model and exhibits  $Z_2$  topological orders. The ground state manifold  $\mathcal{L}$  is given by

$$\{|\psi_g\rangle \in \mathcal{H} : X_p|\psi_g\rangle = Z_p|\psi_g\rangle = |\psi_g\rangle \text{ for all } p\}. \quad (2)$$

The degeneracy of ground states depends on the genus  $g$  of Riemann surface, i.e.,  $D = 2^{2g}$ . If the Riemann surface has genus  $g$ , we can define  $2g$  non-contractible strings that connect different topological sectors in  $\mathcal{L}$ . For example, on a torus its four-fold degenerate ground states can be described by using two nontrivial closed strings of  $\gamma_1$  and  $\gamma_2$ ,

$$|\psi_g^{(\nu_1, \nu_2)}\rangle = \mathcal{T}_x^{\nu_1}(\gamma_1) \mathcal{T}_x^{\nu_2}(\gamma_2) |\psi_g^{(0,0)}\rangle, \nu_1, \nu_2 = 0, 1. \quad (3)$$

Here the string operators are defined as  $\mathcal{T}_x(\gamma) = \prod_{j \in \gamma} \sigma_j^x$ . The initial topological sector  $|\psi_g^{(0,0)}\rangle$  of  $\mathcal{L}$  is given by the equal superposition of all contractible closed strings including no string (or say the string is a point). It is not difficult to find that  $\mathcal{T}_x(\gamma_3) = \prod_{p \in f} X_p$ , namely, the product of all plaquette operators in the surface  $f$  that satisfies  $\partial f = \gamma_3$ . And for no string, its corresponding operator is the identity matrix  $I$ . All operators corresponding to such strings form a group denoted it as  $\mathcal{G}$ . Its elements are generated by  $n = (N^2 - 2)/2$  independent plaquette operators in the white sublattice, i.e.,

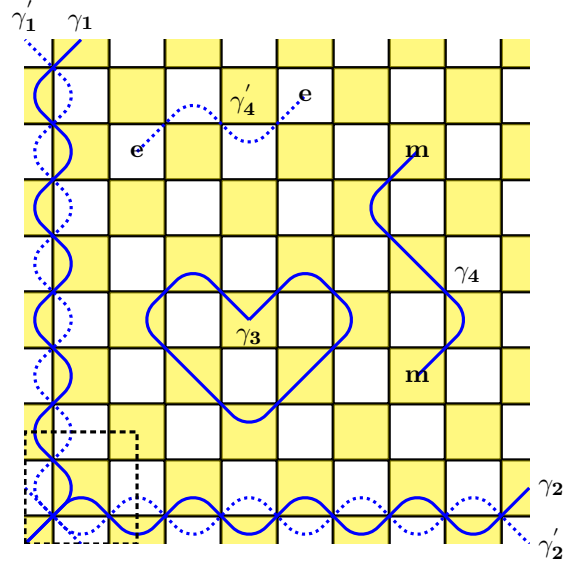


FIG. 1. (Color online) The Wen-plaquette spin-lattice model on a torus. When  $N$  is even, there exist two sublattice denoted by white and yellow. The blue solid strings ( $\gamma_1 \sim \gamma_4$ ) and their dual dashed strings ( $\gamma'_1 \sim \gamma'_4$ ) are defined in the yellow sublattice and in the white sublattice, respectively.  $e$  and  $m$  represent the elementary excitations (anyons): electric charge and magnetic vortex, which in pairs generated by open string operators. The black dashed box is an unit cell of square lattice.

$g_s = \prod_{p=1}^n X_p^{s_p}$ ,  $s_p \in \{0, 1\}$ . Thus,

$$|\psi_g^{(0,0)}\rangle = \frac{1}{\sqrt{|\mathcal{G}|}} \sum_{g_s \in \mathcal{G}} g_s |00 \cdots\rangle, \quad (4)$$

where  $|\mathcal{G}|$  is the number of elements in  $\mathcal{G}$  and  $|0\rangle$  stands for spin-up states along the  $z$  axis. According to the closure of group and the commutation relations, we can prove that  $X_p |\psi_g^{(\nu_1, \nu_2)}\rangle = Z_p |\psi_g^{(\nu_1, \nu_2)}\rangle = |\psi_g^{(\nu_1, \nu_2)}\rangle$  for all  $p, \nu_1, \nu_2$ . Therefore, the states of  $|\psi_g^{(\nu_1, \nu_2)}\rangle$  constructing from Eq. (3) and Eq. (4) are indeed the ground states of Hamiltonian (1). Besides, it shows that  $\langle \psi_g^{(\nu_1, \nu_2)} | \psi_g^{(\nu'_1, \nu'_2)} \rangle = \delta_{\nu_1, \nu'_1} \delta_{\nu_2, \nu'_2}$ , that means, different topological sectors are orthogonal.

An unit cell on a torus is illustrated in Fig. 2, which consists of  $2 \times 2$  spins. Although it is the smallest system, topological orders still exist in the Wen-plaquette spin-lattice model with finite size [20]. This validity also comes from the fairly short-range spin-spin correlations [31]. Under the periodic boundary condition, we can get the Hamiltonian

$$\hat{H}_{\text{Wen}}^4 = -2(X_p + Z_p). \quad (5)$$

Two nontrivial loop operators are  $\mathcal{T}_x(\gamma_1) = \sigma_1^x \sigma_4^x$  and  $\mathcal{T}_x(\gamma_2) = \sigma_1^x \sigma_2^x$  and all contractible closed-string operators form a group, i.e.,  $\mathcal{G} = \{I, X_p\}$ , which are generated

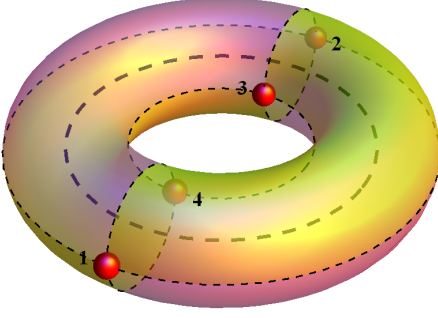


FIG. 2. (Color online) An unit cell of Wen-plaquette model under the periodic boundary condition. The red spheres represent spins.

by one independent plaquette operator, i.e.,  $X_p$ . So from Eq. (3) and Eq. (4), the four-fold degenerate ground states can be described as follows,

$$\begin{aligned} |\psi_g^{(0,0)}\rangle &= (|0000\rangle + |1111\rangle)/\sqrt{2} \\ |\psi_g^{(0,1)}\rangle &= (|0011\rangle + |1100\rangle)/\sqrt{2} \\ |\psi_g^{(1,0)}\rangle &= (|0110\rangle + |1001\rangle)/\sqrt{2} \\ |\psi_g^{(1,1)}\rangle &= (|0101\rangle + |1010\rangle)/\sqrt{2}, \end{aligned} \quad (6)$$

in the  $\sigma_z$  representation. The theory shows that each topological sector in Eq. (6) is maximally entangled state through stochastic local quantum operation assisted by classical communication (SLOCC) [33, 34].

### III. EXPERIMENT

The physical four-qubit system we used in the experiment consists of the nuclear spins in Iodotrifluoroethylene ( $\text{C}_2\text{F}_3\text{I}$ ) molecules with one  $^{13}\text{C}$  and three  $^{19}\text{F}$  nuclei. Figures 3(a) and 3(b) show its molecular structure and relevant parameters. The natural Hamiltonian of this system in the doubly rotating frame is

$$\hat{H}_{\text{NMR}} = \sum_{i=1}^4 \frac{\omega_i}{2} \hat{\sigma}_z^i + \sum_{i<j=1}^4 \frac{\pi J_{ij}}{2} \hat{\sigma}_z^i \hat{\sigma}_z^j, \quad (7)$$

where  $\omega_i$  represents the chemical shift of spin  $i$  and  $J_{ij}$  the coupling constant between spin  $i$  and spin  $j$ . The experiment was carried out on a Bruker AV-400 spectrometer ( $9.4T$ ) at room temperature  $T = 300$  K. The temperature fluctuation was controlled to  $< 0.1$  K, which results in a frequency stability within 1 Hz.

The quantum system was firstly prepared in the initial pseudo-pure state (PPS):  $\hat{\rho}_{0000} = \frac{1-\epsilon}{16} \mathbf{I} + \epsilon|0000\rangle\langle 0000|$  using line-selective approach [35], with  $\mathbf{I}$  representing  $16 \times 16$  identity operator and  $\epsilon \approx 10^{-5}$  the polarization. Note that  $|0000\rangle$  is corresponding to the ground state of  $\hat{H}_0 = -\sum_{j=1}^4 \hat{\sigma}_j^z$ . We then can adiabatically prepare a

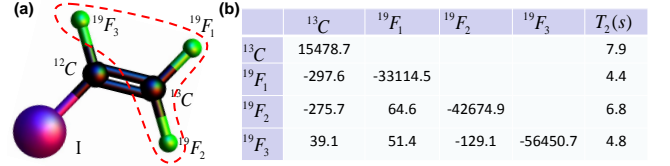


FIG. 3. (Color online.) (a) Molecular structure of Iodotrifluoroethylene. One  $^{13}\text{C}$  and three  $^{19}\text{F}$  nuclei are used as a four-qubit quantum simulator. (b) Relevant parameters measured at  $T = 300\text{K}$ . The diagonal and nondiagonal elements represent the chemical shifts and the coupling constants in units of Hz, respectively. The measured spin-lattice relaxation times ( $T_1$ ) are 21 s for  $^{13}\text{C}$  and 12.5 s for  $^{19}\text{F}$ .

ground state  $|\psi_g^{(0,0)}\rangle$  of Wen-plaquette model by varying the time-dependent Hamiltonian slowly enough,

$$\hat{H}(t) = [1 - s(t)]\hat{H}_0 + s(t)\hat{H}_{\text{Wen}}^4, \quad (8)$$

where the parameter function  $s(t)$  increases monotonically from 0 at  $t = 0$  to 1 at  $t = T$ . The energy levels of  $\hat{H}(t)$  as the function of the parameter  $s(t)$  are shown in Fig. 4(a). The red curve represents the ground-state energy. To ensure that the system always stays in the instantaneous ground state, the variation of the control parameter has to be sufficiently, i.e., the adiabatic condition [36]

$$\frac{\langle \psi_g | \frac{\partial \hat{H}(t)}{\partial s(t)} \frac{\partial s(t)}{\partial t} | \psi_e \rangle}{(\epsilon_e - \epsilon_g)^2} = \epsilon \ll 1, \quad (9)$$

where the index  $e$  represents the excited state. The condition determines the optimal sweep of control parameter  $s(t)$ . The  $s(t)$  was interpolated with  $M$  discretized scan steps and the duration of each step is  $\tau = T/M$ . The adiabatic condition is satisfied when both  $T, M \rightarrow \infty$  and the duration of each step  $\tau \rightarrow 0$ . To determine the optimal number  $M$  of steps in the adiabatic transfer, we used a numerical simulation of the minimum fidelity  $F_{\text{min}}$  encountered during the scan as a function of the number of steps into which the evolution is divided (see Fig. 4(b)), where we fixed the total evolution time  $T = 2.9982$ . The fidelity is calculated as the overlap of the state with the ground state at the relevant position. In the experiment, we discretized into  $M = 7$  steps. Each step had the same duration, i.e.,  $\tau = 0.4282$ . When  $M = 7$ , the minimal fidelity is 0.99, which fully indicates the state of the system is always close to its instantaneous ground state in the whole adiabatic passage.

The adiabatic evolution for each step can be decomposed by Suzuki-Trotter expansion as

$$\begin{aligned} e^{-i\hat{H}[s(l)]\tau} &= e^{-i[1-s(l)]\hat{H}_0\tau/2} e^{-is(l)\hat{H}_{\text{Wen}}^4\tau} \\ &\quad \cdot e^{-i[1-s(l)]\hat{H}_0\tau/2} + O(\tau^3), \end{aligned} \quad (10)$$

with  $l = 0, 1, \dots, M$ . This expansion faithfully represents the targeted evolution provided the duration  $\tau$  is

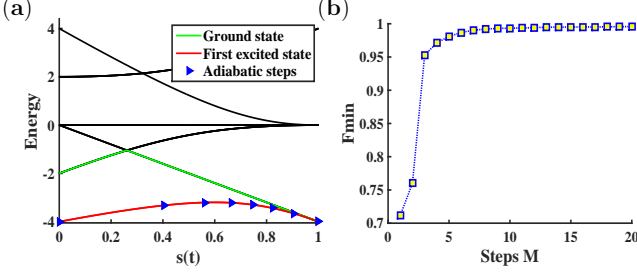


FIG. 4. (Color online) (a) The energy-level diagram of the time-dependent Hamiltonian  $\hat{H}[s(t)]$ . The red and green curves represent the energies of ground state and first excited state, respectively. The blue  $\triangleright$  points represent the  $M = 7$  interpolations on the line of  $s(t)$  with the same time interval  $\tau$ . (b) Numerical simulation of the minimum fidelities during the adiabatic passage vs. the number of steps.

kept sufficiently short. Due to  $[X_p, Z_p] = 0$ , we have

$$e^{-is(l)\hat{H}_{\text{Wen}}^A\tau} = \prod_{j=1}^4 \hat{R}_j^y\left(\frac{\pi}{2}\right) \cdot e^{i2s(l)Z_P\tau} \cdot \prod_{j=1}^4 \hat{R}_j^y\left(-\frac{\pi}{2}\right) \cdot e^{i2s(l)Z_P\tau}. \quad (11)$$

Here the four-body interaction  $Z_P$  is effectively created by a combination of two-body interactions and RF pulses [37, 38]:

$$\begin{aligned} e^{-i2s(l)Z_P\tau} &= \hat{R}_1^z(\theta_1)\hat{R}_2^z(\theta_2)\hat{R}_4^z(\theta_3)\hat{R}_3^y\left(\frac{\pi}{2}\right)e^{-i\hat{H}_{\text{NMR}}\tau_1}\hat{R}_3^y(\pi) \\ &\cdot \hat{R}_4^y(\pi)e^{-i\hat{H}_{\text{NMR}}\tau_1}\hat{R}_1^y\left(-\frac{\pi}{2}\right)\hat{R}_3^x\left(-\frac{\pi}{2}\right)e^{-i\hat{H}_{\text{NMR}}\tau_2} \\ &\cdot \hat{R}_1^y(\pi)\hat{R}_2^y(\pi)e^{-i\hat{H}_{\text{NMR}}\tau_2}\hat{R}_1^x\left(\frac{\pi}{2}\right)e^{-i\hat{H}_{\text{NMR}}\tau_3}\hat{R}_1^x(\pi) \\ &\cdot \hat{R}_3^x(\pi)e^{-i\hat{H}_{\text{NMR}}\tau_3}\hat{R}_1^x\left(\frac{\pi}{2}\right)e^{-i\hat{H}_{\text{NMR}}\tau_2}\hat{R}_1^y(\pi)\hat{R}_2^y(\pi) \\ &\cdot e^{-i\hat{H}_{\text{NMR}}\tau_2}\hat{R}_1^y\left(-\frac{\pi}{2}\right)\hat{R}_3^x(\pi/2)\hat{R}_2^y(\pi)e^{-i\hat{H}_{\text{NMR}}\tau_1} \\ &\cdot \hat{R}_3^x(\pi)\hat{R}_4^x(\pi)e^{-i\hat{H}_{\text{NMR}}\tau_1}\hat{R}_3^y\left(\frac{\pi}{2}\right), \end{aligned} \quad (12)$$

where  $\hat{R}_j^\alpha(\theta) = e^{-i\theta\hat{\sigma}_j^\alpha/2}$  ( $\alpha = x, y, z$ ). Therefore, the adiabatic evolution for each step can be implemented by the pulse sequences, as shown in Figs. 5(a) and 5(b). The simulation method is in principle efficient as long as the decoherence time is long enough. In order to overcome the accumulated pulse errors and the decoherence, we packed the adiabatic passage for each  $s(l)$  ( $l = 0, 1, 2, \dots, M$ ) into one shaped pulse calculated by the gradient ascent pulse engineering (GRAPE) method [39], with the length of each pulse being 30 ms. All the pulses have theoretical fidelities over 0.99, and are designed to be robust against the inhomogeneity of radio-frequency pulses in the experiments.

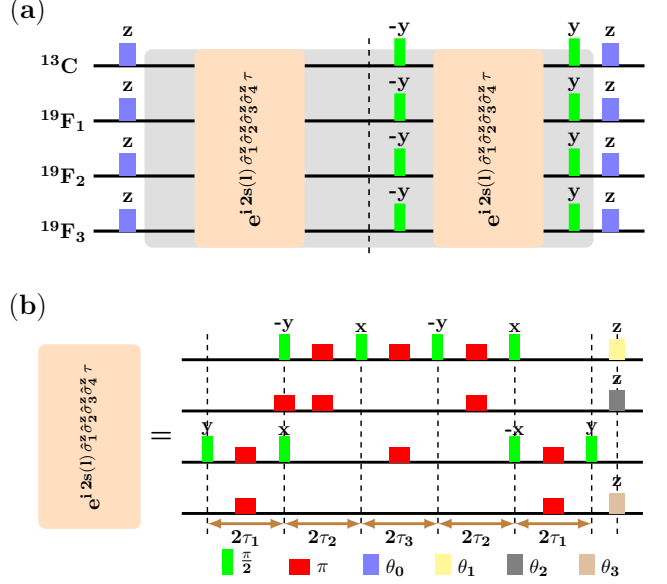


FIG. 5. Pulse sequences for (a) implementing the adiabatic evolution of  $l_{th}$  step, and (b) effectively creating four-body interaction, i.e.,  $\hat{\sigma}_z^1\hat{\sigma}_z^2\hat{\sigma}_z^3\hat{\sigma}_z^4$ , where  $\tau_1 = 1/4J_{34}$ ,  $\tau_2 = 1/4J_{12}$ ,  $\tau_3 = 2s(l)\tau/\pi J_{13}$ ,  $\theta_0 = [1-s(l)]\tau/2$ ,  $\theta_1 = -\omega_1/J_{34}$ ,  $\theta_2 = -4\omega_2s(l)\tau/\pi J_{13}$  and  $\theta_3 = \omega_4/J_{12} + 4\omega_4s(l)\tau/\pi J_{13}$ .

#### IV. RESULTS AND DISCUSSION

Once the initial topologically ordered state  $|\psi_g^{(0,0)}\rangle$  was prepared via the adiabatic evolution, the other topological sectors in  $\mathcal{L}$  were obtained by performing non-contractible string operators  $\mathcal{T}_x^{\nu_1}(\gamma_1)\mathcal{T}_x^{\nu_2}(\gamma_2)$  (taking different values of  $\nu_1, \nu_2$ ) on  $|\psi_g^{(0,0)}\rangle$ . The resulting  $^{13}\text{C}$  spectra for different quantum states are illustrated in Fig. 6, after a readout pulse  $\hat{R}_1^y(\pi/2)$  acting on  $^{13}\text{C}$  observable nucleus. Figure 6 correspond to the spectra of  $|\psi_g^{(0,0)}\rangle$ ,  $|\psi_g^{(0,1)}\rangle$ ,  $|\psi_g^{(1,0)}\rangle$ , and  $|\psi_g^{(1,1)}\rangle$ , respectively. To further confirm the experiments, we reconstructed the quantum state density matrices using the complete tomography technology [40]. For reconstructing a full density matrices of the four-qubit states, we performed 44 independent experiments (see Table. I) to obtain the coefficients of 256 operators, i.e., a complete operator basis of the four-qubit system. In Table. I, this procedure involves 28 local operations and 3 SWAP gates. All of these operations were realized by GRAPE pulses with 400  $\mu\text{s}$  for local operations, 9 ms for the SWAP gates between  $^{13}\text{C}$  and  $F_1$ ,  $F_2$  and 30 ms for the SWAP gate between  $^{13}\text{C}$  and  $F_3$  due to the relatively weak coupling between them. The reconstructed results are shown in Fig. 7, with the fidelities being 96.46%, 96.59%, 96.06% and 96.06% for four topological sectors in  $\mathcal{L}$ , respectively. The receivable fidelities ensure that it is successful to adiabatically prepare the topologi-

TABLE I. Scheme of the reading-out pulses for the quantum state tomography for our four-qubit quantum simulator.  $\text{SWAP}_{ij}$  represents a SWAP gate between spin  $i$  and  $j$  in order to transfer the  $^{19}\text{F}$  information to  $^{13}\text{C}$ , and then all signals are obtained from the  $^{13}\text{C}$  spectra.

EEEE	EYEX	EXXY	EEYX*SWAP <sub>12</sub>
EXEE	EEXX	EYXY	EEEE*SWAP <sub>12</sub>
EYEE	EXXX	EEYY	EEYX*SWAP <sub>12</sub>
EEXE	EYXX	EXYY	EEYY*SWAP <sub>12</sub>
EXXE	EEYX	EYYY	YEEE*SWAP <sub>12</sub>
EYXE	EXYX	YEEE	EEEE*SWAP <sub>13</sub>
EEYE	EYYX	EEEE*SWAP <sub>12</sub>	EEEX*SWAP <sub>13</sub>
EXYE	EEYY	EEEX*SWAP <sub>12</sub>	EEYY*SWAP <sub>13</sub>
EYYE	EXEY	EEYE*SWAP <sub>12</sub>	YEEE*SWAP <sub>13</sub>
EEEX	EYEE	EEEX*SWAP <sub>12</sub>	EEEE*SWAP <sub>14</sub>
EXEX	EEXY	EEXX*SWAP <sub>12</sub>	YEEE*SWAP <sub>14</sub>

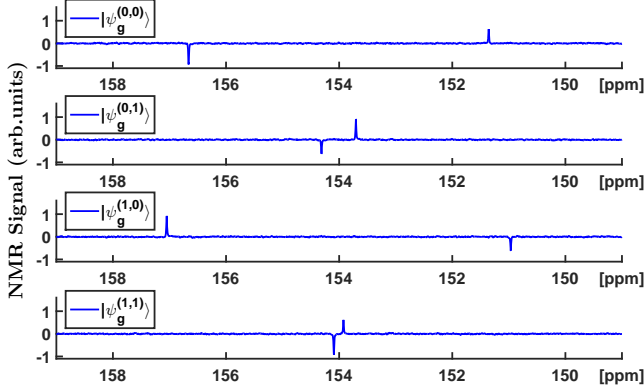


FIG. 6. (Color online) The  $^{13}\text{C}$  spectra corresponding to four topological sectors i.e.,  $|\psi_g^{(0,0)}\rangle$ ,  $|\psi_g^{(0,1)}\rangle$ ,  $|\psi_g^{(1,0)}\rangle$ , and  $|\psi_g^{(1,1)}\rangle$  from top to bottom, respectively.

ical orders with patterns of long-range entanglement.

These experimental results are in good agreement with theoretical expectations. The relatively minor deviations can be attributed mostly to the imperfections of adiabatic approximation, GRAPE pulses and the spectral in-

tegrals. The theoretical infidelities of adiabatic approximation and GRAPE pulses are around 1%. Taking both errors into account, the numerical simulation gives the fidelities of 97.59%, 97.96%, 97.56% and 97.75% for four topological sectors. Though we used the spectral fitting method in the experiments, there are about 1%  $\sim$  1.5% errors from the spectral integrals by the comparison of the simulated and experimental results.

## V. CONCLUSION

The Wen-plaquette spin-lattice model with  $Z_2$  topological order includes four-body interactions, which cannot be found in naturally occurring systems. Quantum simulation provides a powerful means to investigate topological orders. Using an NMR simulator, we realized such model consisting of  $2 \times 2$  lattice on a torus. A topologically ordered state was experimentally prepared through adiabatically engineering the time-dependent Hamiltonian and the other sectors in degenerate ground-state manifold were transferred by performing two non-contractible string operations. The experimental results were confirmed by the complete quantum state tomography. From the reconstructed density matrices, it shows that each topological sector is maximally entangled. The experiment demonstrated the feasibility of adiabatic method to prepare topological orders, which also provides the possibility to further study the topological properties and construct a topological quantum memory.

## VI. ACKNOWLEDGEMENTS

This work is supported by NKBRP(2013CB921800 and 2014CB848700), the National Science Fund for Distinguished Young Scholars (11425523), NSFC(11375167, 11227901 and 91021005), the Strategic Priority Research Program (B) of the CAS(XDB01030400), and RFDP (20113402110044).

- 
- [1] X. G. Wen, Int. J. Mod. Phys. B **4**, 239 (1990).
  - [2] X.-G. Wen, Quantum Field Theory of Many-Body Systems (Oxford University Press, Oxford, 2004).
  - [3] D. C. Tsui, H. L. Stormer, and A. C. Gossard, Phys. Rev. Lett. **48**, 1559 (1982); R. B. Laughlin, *ibid.*, **50**, 1395 (1983).
  - [4] S. Sachdev, *Quantum Phase Transition* (Cambridge University Press, Cambridge 1999).
  - [5] L. D. Landau, Phys. Zs. Sowjet **11**, 26 (1937).
  - [6] V. L. Ginzburg and L. D. Landau, J. Exp. Eheur. Phys. **20**, 1064 (1950).
  - [7] X. Chen, Z. C. Gu, X. G. Wen, Phys. Rev. B **82**, 155138 (2010).
  - [8] A. Kitaev and J. Preskill, Phys. Rev. Lett. **96**, 110404 (2006); M. Levin and X. G. Wen, *ibid.* **96**, 110405 (2006).
  - [9] A. Hamma, W. Zhang, S. Haas, and D. A. Lidar, Phys. Rev. B **77**, 155111 (2008).
  - [10] X.-G. Wen and Q. Niu, Phys. Rev. B. **41**, 9377 (1990).
  - [11] D. Arovas, J. R. Schrieffer and F. Wilczek, Phys. Rev. Lett. **53**, 722 (1984).
  - [12] X. G. Wen, Adv. Phys. **44**, 405 (1995).
  - [13] A. Kitaev, Ann. Phys. (N.Y.) **303**, 2 (2003).
  - [14] C. Nayak *et al.*, Rev. Mod. Phys. **80**, 1083 (2008).
  - [15] A. Stern and N. H. Lindner, Science **339**, 1179-1181 (2013).
  - [16] M. H. Freedman, A. Kitaev, M. J. Larsen, and Z. Wang, Bull. Am. Math. Soc. **40**, 31 (2003).
  - [17] E. Dennis *et al.*, J. Math. Phys. **43**, 4452 (2002).
  - [18] L. Jiang *et al.*, Nat. Phys. **4**, 482-488 (2008).
  - [19] A. Kitaev, Ann. Phys. (N.Y.) **321**, 2(2006).



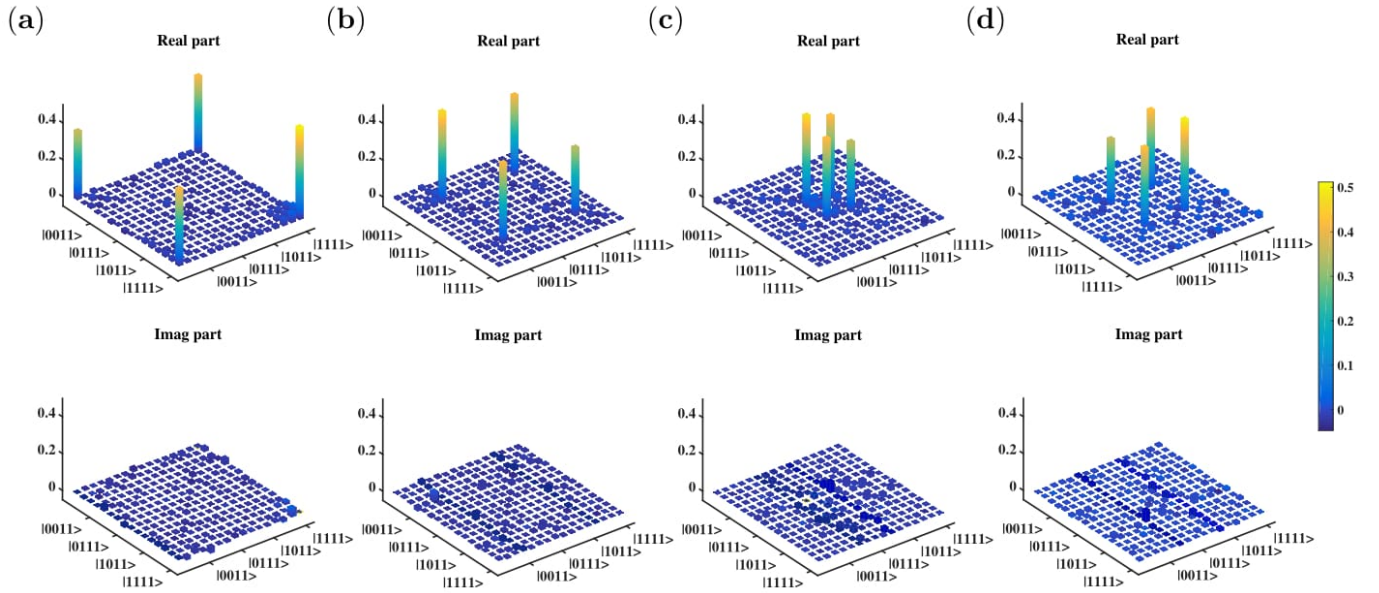


FIG. 7. (Color online) The experimental reconstructed density matrices for different topological sectors, that is,  $|\psi_g^{(0,0)}\rangle$ ,  $|\psi_g^{(0,1)}\rangle$ ,  $|\psi_g^{(1,0)}\rangle$ , and  $|\psi_g^{(1,1)}\rangle$  corresponding to (a)~(d), respectively. The top and bottom represent the real parts and imaginary parts.

- [20] X. G. Wen, Phys. Rev. Lett. **90**, 016803 (2003).
- [21] R. P. Feynman, Int. J. Theor. Phys. **21**, 467 (1982).
- [22] A. Friedenauer, H. Schmitz, J. T. Glueckert, D. Porras, and T. Schaetz, Nature Phys. **4**, 757 (2008).
- [23] J. Clarke and F. K. Wilhelm, Nature (London) **453**, 1031 (2008).
- [24] L. M. K. Vandersypen and I. L. Chuang, Rev. Mod. Phys. **76**, 1037 (2005).
- [25] X. C. Yao *et al.*, Nature **482**, 489-494 (2012); C. Y. Lu *et al.*, Phys. Rev. Lett. **102**, 030502 (2009); J. K. Pachos *et al.*, New. J. Phys. **11**, 083010 (2009).
- [26] J. F. Du, J. Zhu, M. G. Hu, and J. L. Chen, arXiv:0712.2694v1 (2007); G. R. Feng, G. L. Long, and R. Laflamme, Phys. Rev. A **88**, 022305 (2013).
- [27] X. H. Peng, J. F. Du, and D. Suter, Phys. Rev. A **71**, 012307 (2005); K. Kim *et al.*, Nature **465**, 590 (2010); X. H. Peng, J. F. Zhang, J. F. Du and D. Suter, Phys. Rev. Lett. **103**, 140501 (2009); Gonzalo A. Álvarez and Dieter Suter, Phys. Rev. Lett. **104**, 230403 (2010).
- [28] J. F. Du *et al.*, Phys. Rev. Lett. **104**, 030502 (2010); B. P. Lanyon *et al.* Nat. Chem. **2** 106 (2010); D. W. Lu *et al.*, Phys. Rev. Lett. **107**, 02050 (2011).
- [29] I. M. Georgescu, S. Ashhab and F. Nori, Rev. Mod. Phys. **86**, 153 (2014).
- [30] A. Hama and D. A. Lidar, Phys. Rev. Lett. **100**, 030502 (2008).
- [31] X. H. Peng, Z. H. Luo, W. Q. Zheng, S. P. Kou, D. Suter, and J. F. Du, Phys. Rev. Lett. **113**, 080404 (2014).
- [32] Z. H. Luo, J. Li, Z. K. Li, Y. D. W, L. X. Hung, X. H. Peng, and J. F. Du, *Identifying topological order by measuring the modular S and T matrices*, in preparation (2016).
- [33] F. Verstraete, J. Dehaene, B. De Moor, and H. Verschelde, Phys. Rev. A. **65**, 052112 (2002).
- [34] B. Regula, S. D. Martino, S. Lee, and G. Adesso, Phys. Rev. Lett. **113**, 110503 (2014).
- [35] X. Peng, X. Zhu, X. Fang, M. Feng, K. Gao, X. Yang, and M. Liu, Chem. Phys. Lett. **340**, 509 (2001).
- [36] Messiah, A. *Quantum Mechanics* (Wiley, New York, 1976).
- [37] C. H. Tseng, et al, Phys. Rev. A **61**, 012302 (1999).
- [38] X. H. Peng, J. F. Zhang, J. F. Du and D. Sutter, Phys. Rev. Lett **103**, 140501 (2009).
- [39] Khaneja, N., Reiss, T., Kehlet, C., Schulte Herbrüggen, T. & Glaser, S. J., J. Magn. Reson **172**, 296 (2005).
- [40] J. S. Lee, Phys. Lett. A **305**, 349-353 (2002).